Water Quality Simulation of Reclaimed Water Supply Type Rivers and Application of Metal Organic Frameworks in Phosphorus Pollution Control

Qunbo QIAO [1], Mingxiang ZHANG [1] *, Bingyi HAN [2], Weihua WANG [3]

[1] *School of Ecology and Nature Conservation, Beijing Forestry University, Beijing 100083, China*
[2] *College of Environmental Science and Engineering, Beijing Forestry University, Beijing 100083, China*
[3] *Beijing Beikong Industrial Environmental Technology Co., Ltd, Beijing 101407, China*

http://doi.org/10.5755/j02.ms.41345

Received 29 April 2025; accepted 9 June 2025

This study focuses on the Xinfeng River, a regenerated water supply type river, and conducts water quality simulation and research on the application of metal organic framework materials (MOFs) in phosphorus pollution control. Using the storm water management model (SWMM) and environmental fluid dynamics code (EFDC) coupling model, the water quality changes of Xinfeng River under different scenarios of reclaimed water supply were simulated. The model was calibrated and verified through historical monitoring data, and the results showed that chemical oxygen demand (COD) could stably meet the Class V water quality standard, while NH_3-N and total phosphorus (TP) could not meet the standard. Secondly, NH_2-MIL-125(Ti) and NH_2-UIO-66(Zr) were synthesized in this study. The morphology, structure, and properties of MOFs were characterized using scanning electron microscopy (SEM), Fourier transform infrared spectroscopy (FTIR), X-ray diffraction (XRD), Brunauer-Emmett-Teller (BET), and thermogravimetric analysis (TGA), and they were used for adsorption and removal of phosphorus in water environments. The results indicate that NH_2-MIL-125(Ti) has a larger adsorption capacity (10.42 mg/g), and the adsorption of phosphorus by NH_2-MIL-125(Ti) and NH_2-UIO-66(Zr) is more in line with the quasi second order kinetic model, and their adsorption isotherms are more in line with the Freundlich model. In addition, both adsorbents have good adsorption regeneration performance, with a phosphorus removal rate of over 85 % after 5 cycles. The water quality simulation model constructed in this study can accurately predict the impact of recycled water supply on river water quality. The selected MOFs materials have good phosphorus adsorption and removal performance, providing a scientific basis and technical support for improving water quality and controlling phosphorus pollution in recycled water supply rivers.

Keywords: regenerated water supply type river, water quality simulation, organic framework materials, adsorbent, phosphorus removal.

1. INTRODUCTION

Global water scarcity has become one of the most severe environmental challenges of the 21st century. According to the UNESCO World Water Development Report 2023, approximately 40 % of the global population is currently facing varying degrees of water resource pressure, and this proportion may rise to 60 % by 2030. Therefore, the strategic value of reclaimed water as a "second water source" is increasingly prominent [1]. Especially in urban watershed management, recycled water supply has become an important way to maintain the ecological base flow of rivers [2]. According to statistics, the proportion of recycled water supply in rivers in some cities in northern China has exceeded 30 %, and even reaches over 70 % during dry seasons [3]. However, while the supply of recycled water can alleviate water scarcity, it also brings water quality risks, especially excessive nitrogen and phosphorus [4, 5]. The conventional sewage treatment process has limited removal efficiency for nutrients such as nitrogen and phosphorus, resulting in a total phosphorus (TP) concentration in recycled water typically maintained at 0.3 – 1.0 mg/L (higher than the Class III standard limit of 0.2 mg/L for surface water). When such recycled water continues to be input into river systems, it may cause a series of water environmental problems [6]. Research has shown that the cumulative effect of phosphorus in rivers supplied with recycled water can increase the growth rate of algae by 3 – 5 times, significantly increasing the risk of eutrophication in water bodies [7, 8]. More complexly, under dynamic hydrological conditions, riverbed sediments will form a "phosphorus sink source" conversion mechanism [9], making it difficult for traditional water quality models to accurately predict the migration and transformation patterns of phosphorus.

Many studies have been conducted by scholars from various countries on water quality simulation of rivers supplied with recycled water [10, 11]. Some scholars have studied pollutant migration simulations based on mechanistic models such as the water quality analysis simulation program (WASP) and QUAL2K. By improving the Monod equation parameters in the kinetic model [12], the accuracy of describing nutrient cycling processes has been enhanced. Some scholars also focus on the application of data-driven models. Barzegar et al. [13] developed two standalone deep learning (DL) models, the long short-term memory (LSTM) and convolutional neural network (CNN) models, along with their hybrid, the CNN-LSTM model.

* Corresponding author: M. Zhang
E-mail: *zhangmingxiang@bjfu.edu.cn*

They built a coupled CNN-LSTM model to predict water quality variables. Two traditional machine learning models, support-vector regression (SVR) and decision tree (DT), were also developed to compare with the DL models. In addition, more scholars are interested in the research of multi-scale modeling methods. Different dimensional coupled models are often constructed based on the characteristics of the research object and purpose, and have stronger applicability [14, 15]. Hwang et al. [16] coupled the watershed soil and water assessment tool (SWAT) model with the river environmental fluid dynamics code (EFDC) model for simulating river water quality. They evaluated the effects of water quality management on the estuarine reservoir, which is separated by levees, using the SWAT- EFDC linkage model. Kadam et al. [17] used a one-dimensional MIKE11 model and a two-dimensional MIKE21 model coupled to simulate flood inundation in the Ahoi River floodplain.

For the problem of excessive TP content in recycled water, appropriate methods need to be adopted for its treatment. Traditional phosphorus removal techniques mainly include chemical precipitation (aluminum/iron salt addition) [18], biological enhancement (EBPR process) [19], and artificial wetlands [20]. However, these technologies face significant limitations when applied to recycled water supply scenarios, where chemical precipitation methods generate a large amount of sludge (increasing treatment costs by 15 – 20 %), and biological methods have strict requirements for carbon to phosphorus ratio (C/P) (usually > 20). In recent years, adsorption methods have attracted attention due to their advantages of simple operation and renewability [21], among which metal organic framework materials (MOFs) have shown great potential for application [22]. MOFs have ultra-high specific surface area (up to 7000 m^2/g), and their pore structure can be designed [23]. At present, some studies have reported on the application of MOFs in phosphorus adsorption. Xie et al. [24] prepared iron-based MOFs, namely MIL-101 and NH_2-MIL-101, using a universal and simple strategy. They studied the performance of these two MOFs as phosphate removal adsorbents and analyzed the effects of various factors on phosphate adsorption, including adsorbent dosage, contact time, and coexisting ions. Wu et al. [25] synthesized MIL-101(Fe), MIL-101, and graphene oxide (GO)/MI-101(Fe, Cu), and compared the adsorption performance of these three MOF based composite materials in removing phosphate. They found that the adsorption mechanism of phosphate is electrostatic attraction, forming coordination bonds and hydrogen bonds.

Although there have been some studies on water quality simulation of rivers with recycled water supply, existing water quality models rarely consider the multi process coupling effect of recycled water supply, river hydrology, and water quality. For example, how does the fluctuation of supply flow affect the changes in N, P, and chemical oxygen demand (COD) concentrations in rivers? The lack of clarity in this mechanism will result in significant prediction bias of the model under sudden hydrological conditions. In addition, the MOFs materials developed in the laboratory face issues such as wide pH adaptability and structural stability when adsorbing and removing phosphorus pollutants from actual water bodies. Therefore, this article takes the Xinfeng River (Daxing District, Beijing), a river that is supplied with recycled water, as the research object, and conducts water quality simulation research based on a coupled model to reveal the impact of recycled water supply on river water quality. Meanwhile, efficient functionalized MOFs materials, namely NH_2-MIL-125(Ti) and NH_2-UIO-66(Zr), were screened and synthesized to investigate their application performance in phosphorus pollution control. This article aims to provide a scientific basis and technical support for water quality management and phosphorus pollution control of rivers supplied with recycled water, and promote the safe and sustainable application of recycled water in the field of ecological water replenishment in rivers.

2. MATERIALS AND METHODS

2.1. Construction of the coupled watershed hydrology-hydrodynamics-water quality model

A cross-platform coupling framework that links storm water management model (SWMM) 5.0 and EFDC is established, and the technical workflow is depicted in Fig. 1. The SWMM 5.0 engine is written in C, and its computational core is encapsulated in the dynamic-link library SWMM5.dll, which permits distributed storage of input files and executables. By contrast, EFDC is implemented in Fortran and without source-code modification requires that its input files reside in the same physical directory as EFDC.exe. The heterogeneity between these two programming environments presents significant integration challenges. To overcome them, we devised a three-layer interaction mechanism implemented in Python, exploiting Python's "glue" capabilities to achieve seamless coupling of the disparate models.

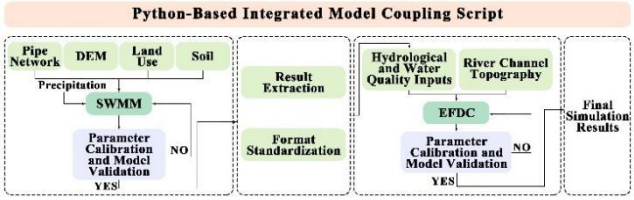

Fig. 1. Technical route map of the integrated model coupling

During the development of the SWMM driver module, SWMM5.dll was loaded via the PySWMM 1.3.2 library to establish an in-memory data channel. While the model advanced at 5 min intervals, flow rates (m^3/s) and water-quality variables COD and NH_3-N concentrations were captured for 24 sub-catchments, yielding continuous time-series datasets. Implemented with a generator pattern, the module achieved a data-capture efficiency of 98.7 % and minimised memory overhead. A data-conversion layer, designed in strict accordance with the EFDC.inp specification, translated SWMM sewer-network outputs into riverine boundary conditions, with dedicated handling of 21 storm outfalls and two inter-basin water-transfer works. Model scheduling was orchestrated with Python's subprocess module: once EFDC input files were generated, the script automatically invoked EFDC.exe through the command line. A file-locking mechanism

ensured temporal synchronisation SWMM output at time *t* immediately triggered EFDC computation at *t*+1. Checkpoint logging enables fault-tolerant restarts, allowing the simulation to resume from the most recent complete time-step after any interruption and thereby enhancing robustness. Benchmark tests demonstrated successful alignment of SWMM's minute-scale steps with EFDC's 15 min steps, with data-transfer latency kept below 200 ms. Relative to conventional file-exchange approaches, the coupled framework improved computational efficiency by 4.2 × and reduced memory usage by 65 %. These advances surmount long-standing C/Fortran integration barriers and furnish a reusable pathway for multi-scale water-environment simulations. The core algorithms have been released as an open-source toolkit CoupleSWMM-EFDC v1.0 supporting ross-platform deployment on both Windows and Linux and providing technical support for integrated basin-scale modelling.

2.2. Conceptualization of the reclaimed water supplementation project model

According to the Integrated Rehabilitation and Ecological Corridor Connectivity Plan for the Xinfeng River Basin in Daxing District, Beijing, six water-supplementation reaches have been engineered within the basin (Fig. 2).

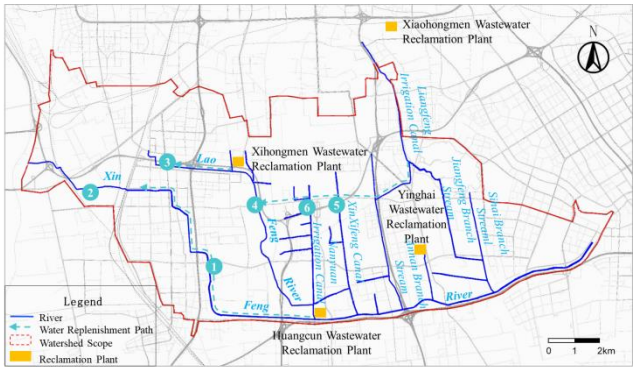

Fig. 2. Schematic diagram of the water system connectivity project

The designated reach names and their respective design inflow rates are as follows:

1) Huangcun Reclaimed-water Plant at the Taiwan Street culvert outlet (1.5×10^4 m^3/d); 2) Huangcun Reclaimed-water Plant at the Liying Sluice (2.5×10^4 m^3/d); 3) Xihongmen Reclaimed-water Plant at the Laofeng River (2.7×10^4 m^3/d); 4) Xiaohongmen supplemental flow to the Laofeng River (including the Tuanhe Imperial Residence section) (6.0×10^4 m^3/d); 5) Xin Xifeng River diversion (0.77×10^4 m^3/d); 6) Nanyuan Irrigation Canal diversion (0.96×10^4 m^3/d).

Based on the foregoing description of the supplementation projects, a boundary-condition table was compiled that specifies, for each reach, the design inflow rate together with the corresponding reclaimed-water quality parameters. Because all supplemental flows originate from wastewater-treatment-plant effluents, long-term monitoring data confirm that their quality consistently meets and indeed surpasses the limits prescribed by Beijing Local Standard B for reclaimed-water discharge (Table 1).

2.3. Synthesis and characterization of adsorbents

2.3.1. Chemical reagents

The specifications of the chemicals used in this work are summarized in Table 2.

2.3.2. Synthesis of NH_2-MIL-125(Ti)

H_2BDC-NH_2 (1.449 g, 8 mmol) was dissolved in 30 mL of a 1:1(v/v) N,N-dimethylformamide (DMF)/methanol mixture and stirred for 10 min at ambient temperature. 1.39 mL titanium isopropoxide (1.308 g, 4.5 mmol) was then added dropwise under continuous stirring. The resulting solution was transferred to a Teflon-lined stainless-steel autoclave, sealed, and heated at 150 ℃ for 16 h. After the reaction, the autoclave was cooled to room temperature, and the yellow precipitate was isolated by filtration, washed successively with DMF and methanol, and dried overnight under vacuum at 60 ℃ to afford the target product.

2.3.3. Synthesis of NH_2-UIO-66(Zr)

$ZrCl_4$ (0.240 g) and 2-aminoterephthalic acid (0.186 g) were dispersed in 60 mL of DMF and vigorously stirred in a 100 mL Teflon-lined autoclave.

Table 1. Boundary conditions for the design of the water supply project

Water source for replenishment	Replenishment location	Design replenishment volume, 10^4 m^3/d	Flow boundary, m^3/s	COD, mg/L	NH_3-N, mg/L	TP, mg/L
Huangcun reclaimed water plant	Taiwan street	1.5	0.174	20	0.5	0.3
Huangcun reclaimed water plant	Liying sluice	2.5	0.289	20	0.5	0.3
Xihongmen reclaimed water plant	Laofeng river	2.7	0.313	20	0.5	0.3
Xiaohongmen reclaimed water plant	Laofeng river	4.27	0.494	20	0.5	0.3
Xiaohongmen reclaimed water plant	Xin xifeng river	0.77	0.089	20	0.5	0.3
Xiaohongmen reclaimed water plant	Nanyuan irrigation canal	0.96	0.111	20	0.5	0.3
Total		12.7				

Table 2. Brief description of the used chemicals

Name	Abbreviation	CAS registry number	Mass fraction purity	Molecule weight	Supplier
2-Aminoterephthalic Acid	H_2BDC-NH_2	10312-55-7	>0.98	181.146	Aladdin
Dimethylformamide	DMF	68-12-2	>0.98	73.09	Aladdin
Methanol	MeOH	67-56-1	>0.99	32.04	Aladdin
Titanium isopropoxide	TTIP	546-68-9	>0.98	284.22	Aladdin
Zirconium tetrachloride	$ZrCl_4$	10026-11-6	>0.99	233.036	Aladdin

The sealed reactor was heated at 120 ℃ for 24 h. After cooling to ambient temperature, the solid was isolated and washed repeatedly with fresh DMF to remove unreacted precursors, followed by solvent exchange with methanol to displace DMF from the pores. The material was then dried under vacuum at 100 ℃ to eliminate residual solvents, affording the final product.

2.3.4. Characterization

The surface morphology of the adsorbent was examined using scanning electron microscopy (SEM; MIRA LMS, TESCAN, Czech Republic). Surface functional groups were identified by Fourier transform infrared spectroscopy (FTIR; Spectrum Two, PerkinElmer, USA). Crystalline structure was probed via X-ray diffraction (XRD; Ultima IV, Rigaku, Japan). Specific surface area was determined from N_2-adsorption isotherms on a Brunauer-Emmett-Teller (BET) surface-area and porosity analyser (ASAP 2460, Micromeritics, USA). Thermal stability was evaluated by thermogravimetric analysis (TGA; STA 200, Hitachi, Japan).

2.4. Evaluation of phosphate adsorption performance of amino-functionalized MOFs

A series of phosphate solutions of known concentration were prepared, and the initial pH was adjusted with 0.5 mol/L HCl or NaOH. The synthesized NH_2-MIL-125(Ti) or NH_2-UIO-66(Zr) sorbent was then added to each solution, which was agitated at 150 r/min in an isothermal shaker held at 25 ℃. Samples were withdrawn at predetermined intervals (0, 0.1, 0.25, 0.5, 1, 2, 5, 7, 10, and 12 h) to determine the residual phosphate concentration. The effects of contact time and initial pH (3, 4, 5, 6, 7, 8, 9, 10, and 11) on adsorption behaviour were systematically investigated, enabling a comparative assessment of the two metal-organic frameworks with respect to phosphate removal efficiency.

The phosphorus adsorption capacity of the adsorbent was calculated according to the Eq. 1:

$$q_e = \frac{(C_0 - C_e) \times V}{m}, \quad (1)$$

where q_e is the amount of phosphorus adsorbed per unit mass of adsorbent at equilibrium, mg/g; C_0 and C_e denote the phosphate concentrations before and after adsorption, respectively, mg/L; V is the volume of the solution, L; m is the mass of adsorbent used, mg.

The experimental data were fitted and compared using pseudo-first-order and pseudo-second-order kinetic models.

To investigate the adsorption isotherms, ten portions of 0.05 g NH_2-MIL-125(Ti) (or NH_2-UIO-66(Zr)) were each added to 100 mL phosphate solutions with initial concentrations of 1, 2, 5, 10, 15, 20, 30, 50, 70, and 100 mg/L, respectively. All mixtures were agitated in a thermostatic shaker at 25 ℃ and 150 r/min for 12 h to ensure equilibrium. The equilibrium concentrations were then measured. The resulting data were subjected to regression analysis using the Freundlich and Langmuir isotherm models to evaluate the adsorption capacities and mechanistic differences between the two MOFs in phosphate removal.

2.5. Adsorption-desorption regeneration experiments

0.05 g NH_2-MIL-125(Ti) (or NH_2-UIO-66(Zr)) was added to a 5 mg/L phosphate solution and agitated at 150 r/min in a thermostatic shaker at 25 ℃ for 12 h. After adsorption, the residual phosphate concentration in the solution was measured. The spent adsorbent was then separated and regenerated using 0.1 mol/L sodium hydroxide solution, and subsequently reused in the next adsorption cycle. This adsorption-desorption process was repeated multiple times to assess the variation in phosphate removal efficiency after successive regeneration cycles. Phosphate concentrations in solution were determined using the molybdenum blue spectrophotometric method.

3. RESULTS AND DISCUSSION

3.1. Simulation results of the reclaimed water supplementation project

After comprehensive water quality management, the the river water data in 2019 can better reflect the impact of water replenishment projects on water quality, as well as the dynamic changes in water quality under engineering interventions. Therefore, the year-round water quality dynamics at the Shaobingzhuang Sluice cross-section of the Xinfeng River in 2019 were simulated under the influence of water-supplementation projects. The temporal variations in water quality were further analyzed across different periods namely, the rainy season, the non-rainy season-winter, and the non-rainy season-other months. The variations in COD, NH_3-N, and TP concentrations at the Shaobingzhuang section are shown in Fig. 3, while the spatial distribution of COD, NH_3-N, and TP concentrations across the entire basin during the non-rainy season is illustrated in Fig. 4.

Water quality monitoring data at the Shaobingzhuang Sluice section indicate that under Class IV water quality standards, the compliance rate for COD concentrations was only 1.6 % on a monthly basis. No compliance was observed during December to February of the following year, as well as in March-May and September-November; the compliance rate during June-August was merely 5.6 %. Under the more lenient Class V standard, the annual compliance rate for COD reached 97.5 %, with full compliance observed in December-February, March-May, and September-November, and a 91.6 % compliance rate during June-August. In contrast, NH_3-N and TP concentrations failed to meet both Class IV and V standards throughout the year. Following the implementation of the reclaimed water supplementation project, the annual COD load was reduced by 56.8 t. Of this, 10.1 t was eliminated during December-February, 23.3 t during March-May and September-November combined, and 23.4 t during June-August. The annual NH_3-N load reduction totaled 125 t, with respective seasonal reductions of 35.7 t (December-February), 49.4 t (March-May and September-November), and 39.8 t (June-August). For TP, the total annual reduction was 12.4 t, distributed as 3.6 t (December-February), 4.9 t (March-May and September-November), and 3.9 t (June-August).

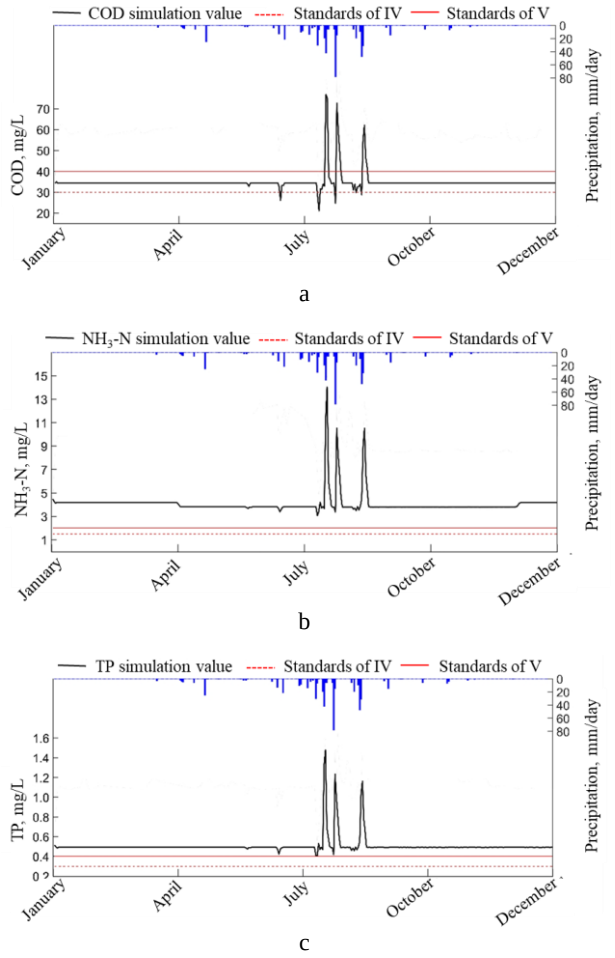

Fig. 3. Annual simulation diagram of water quality concentration dynamics at the section of Shaobingzhuang sluice in the water supply project: a – COD; b – NH_3-N; c – TP

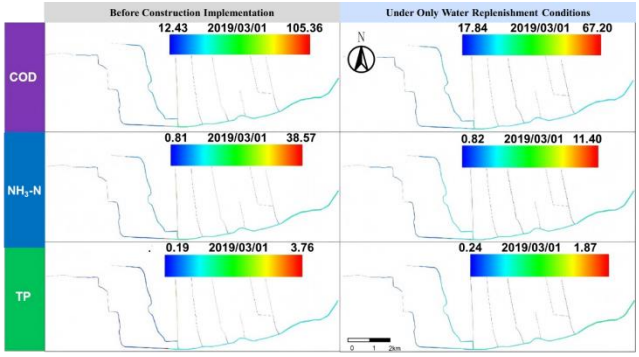

Fig. 4. Spatial distribution map of the concentration of water quality pollutants in the entire basin during the non-rainy season under the condition of water replenishment

Reclaimed water supplementation can, to a certain extent, dilute existing pollutants and help maintain ecological flow levels. However, when evaluated solely from the perspective of the water-supplementation project itself, only COD at the Shaobingzhuang Sluice section consistently meets the Class V water quality standard, while NH_3-N and TP remain non-compliant. Relying exclusively on supplementation measures is insufficient to ensure that the monitored cross-section at the downstream end of the main river channel meets Class IV or V standards. Additional interventions targeting NH_3-N and TP in the water body are therefore necessary. Therefore, the present study investigates the phosphate adsorption performance of amino-functionalized MOFs as a potential solution.

3.2. Characterization of adsorbents

3.2.1. SEM

The SEM images of NH_2-MIL-125(Ti) and NH_2-UIO-66(Zr) are presented in Fig. 5. NH_2-MIL-125(Ti) exhibits a relatively uniform cylindrical particle morphology, with an average diameter of approximately 500 nm.

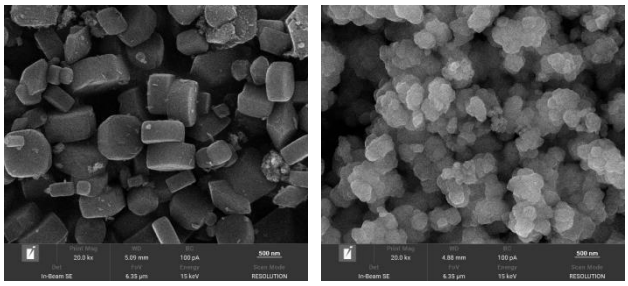

a b

Fig. 5. The SEM image: a – NH_2-MIL-125(Ti); b – NH_2-UIO-66(Zr)

The particle surfaces appear smooth, free from large protrusions or depressions, and show no signs of aggregation. In contrast, NH_2-UIO-66(Zr) displays a polyhedral particle morphology, with significantly smaller particle sizes ranging from several tens to a few hundred nanometers. This smaller and more regular morphology contributes to a higher specific surface area, thereby enhancing the material's adsorption capacity. Furthermore, the surface of NH_2-UIO-66(Zr) features numerous pores with uneven size and distribution. These interconnected pores form a complex porous network, providing accessible channels and sufficient space for phosphate ion diffusion and adsorption. As a result, NH_2-UIO-66(Zr) demonstrates favorable phosphate removal performance.

3.2.2. FTIR

The FTIR spectra of NH_2-MIL-125(Ti) and NH_2-UIO-66(Zr) are shown in Fig. 6. For NH_2-MIL-125(Ti) (Fig. 6 a), distinct absorption peaks are observed in the range of 3300~3500 cm^{-1}, corresponding to the asymmetric and symmetric stretching vibrations of the N-H bonds in amino groups.

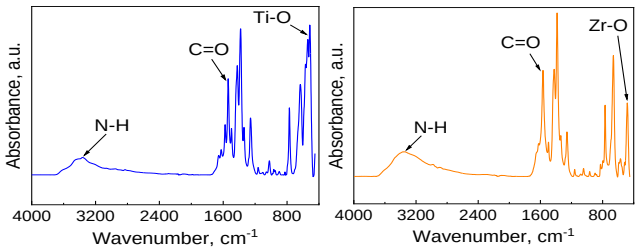

Fig. 6. The FTIR spectra: a – NH_2-MIL-125(Ti); b – NH_2-UIO-66(Zr)

These are characteristic peaks of amino functionalities, confirming the successful incorporation of -NH_2 groups into

the framework. The presence of amino groups, known for their high reactivity, enhances adsorption performance by interacting with phosphate ions through electrostatic attraction or coordination. An absorption band at approximately 1600 cm^{-1} is assigned to the stretching vibration of the C=O bonds in carboxyl groups. Additionally, absorption peaks in the range of 400 ~ 600 cm^{-1} are attributed to Ti-O stretching vibrations, a hallmark of the MIL-125(Ti) framework. These Ti-O bonds are essential for maintaining the material's structural stability and integrity. In the case of NH_2-UIO-66(Zr) (Fig. 6 b), similar N-H stretching vibration bands are observed near 3300 ~ 3500 cm^{-1}, indicating the presence of surface amino groups, which offer abundant active sites for interaction with phosphate ions and contribute significantly to adsorption capacity. A strong absorption peak around 1600 cm^{-1} corresponds to the characteristic vibration of the carboxyl group. Peaks appearing in the 450 ~ 600 cm^{-1} region are attributed to Zr-O stretching vibrations, which are indicative of the Zr-O framework in UIO-66(Zr). This robust zirconium-oxygen network imparts high structural stability and rigidity, ensuring the integrity of the material during the adsorption process.

3.2.3. XRD

XRD is a powerful technique for characterizing the crystalline structure of materials. The XRD patterns of NH_2-MIL-125(Ti) and NH_2-UIO-66(Zr) are shown in Fig. 7.

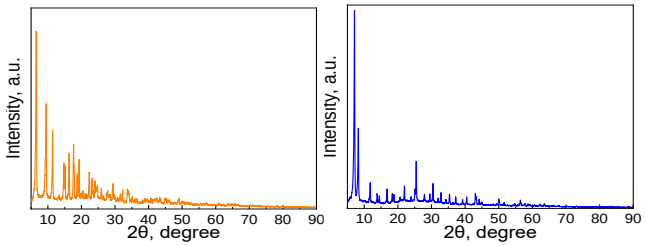

Fig. 7. The XRD patterns: a – NH_2-MIL-125(Ti); b – NH_2-UIO-66(Zr)

For NH2-MIL-125(Ti), distinct diffraction peaks appear at 2θ values of 6.8°, 9.8°, 12.1°, 17.3°, and 18.8°, which are consistent with the standard diffraction pattern of MIL-125(Ti), indicating that the synthesized material possesses a well-defined MIL-125(Ti) crystalline structure. Similarly, the XRD pattern of NH2-UIO-66(Zr) exhibits prominent peaks at 2θ values of 7.3°, 8.2°, 12.4°, and 24.8°, which align well with the standard pattern of UIO-66(Zr). This confirms that the synthesized material exhibits the characteristic crystalline structure of UIO-66(Zr).

3.2.4. BET

The nitrogen adsorption-desorption isotherms of NH_2-MIL-125(Ti) and NH_2-UIO-66(Zr) measured at 77 K are shown in Fig. 8. For NH_2-MIL-125(Ti), the BET method was applied to calculate a specific surface area of 1218.6 m^2/g. This high surface area is attributed to its three-dimensional porous framework, in which the coordination between titanium ions and organic ligands forms a structure rich in both micropores and mesopores. These abundant pores provide ample surface area and internal space for nitrogen adsorption, resulting in the material's high BET surface area. The adsorption isotherm of NH_2-MIL-125(Ti) is typically classified as Type IV, characteristic of mesoporous materials.

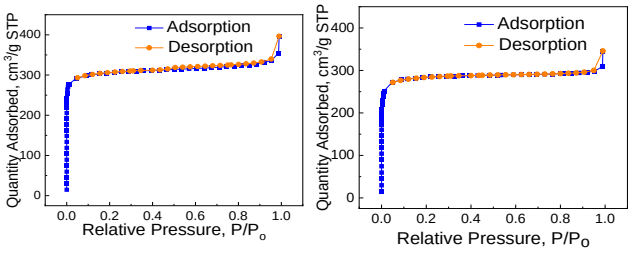

Fig. 8. The BET spectra: a – NH_2-MIL-125(Ti); b – NH_2-UIO-66(Zr)

Similarly, NH_2-UIO-66(Zr) also exhibits a high specific surface area of 1145.0 m^2/g. This is ascribed to its unique crystalline architecture, composed of octahedral secondary building units formed by zirconium ions and carboxylate linkers, which assemble into a porous framework capable of effectively adsorbing gas molecules. The substantial surface areas of both NH_2-MIL-125(Ti) and NH_2-UIO-66(Zr) thus provide a solid foundation for their application in phosphate adsorption and removal.

3.2.5. TGA

TGA is a crucial technique for evaluating the thermal stability of materials. The TGA curves of NH_2-MIL-125(Ti) and NH_2-UIO-66(Zr) are presented in Fig. 9.

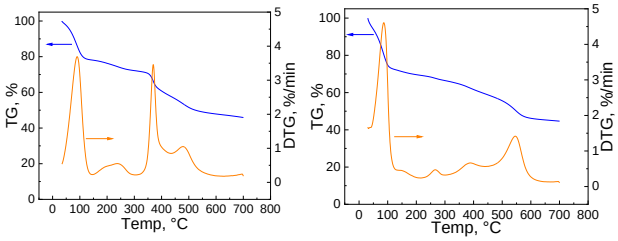

Fig. 9. The TGA spectra: a – NH_2-MIL-125(Ti); b – NH_2-UIO-66(Zr)

For NH_2-MIL-125(Ti), a slight mass loss is observed at temperatures below 200 °C, primarily attributed to the desorption of physically adsorbed water molecules and other volatile surface impurities. As the temperature increases, a significant weight loss occurs between 350 – 500 °C, corresponding to the decomposition of the organic ligands and the gradual breakdown of coordination bonds between the ligands and titanium ions. Beyond 500 °C, the rate of weight loss slows down, and the material enters a relatively stable high-temperature phase. At this stage, the remaining inorganic residues, mainly titanium oxides, are thermally stable, with only minor mass loss observed at elevated temperatures. For NH_2-UIO-66(Zr), a similar low-temperature mass loss is seen below 200 °C due to the desorption of surface-bound species. Between 200 and 500 °C, the material undergoes a more pronounced weight loss as partial decomposition of functional groups within the organic ligands occurs, and coordination with

zirconium ions weakens. When the temperature exceeds 500 ℃, the degradation rate accelerates noticeably, resulting from the substantial decomposition of organic linkers and the progressive collapse of the crystalline structure. Above 600 ℃, the mass loss tends to stabilize, with the remaining residue primarily consisting of zirconium oxide. The minimal weight change at this stage is likely due to the complete combustion of residual organics or minor structural rearrangements within the inorganic framework. Overall, both NH_2-MIL-125(Ti) and NH_2-UIO-66(Zr) exhibit good thermal stability, retaining structural integrity to a considerable extent under high-temperature conditions.

3.3. Analysis of phosphate adsorption performance

The pH value plays a crucial role in influencing the phosphate adsorption performance of NH_2-MIL-125(Ti) and NH_2-UIO-66(Zr). In this study, under conditions of an initial phosphate concentration of 5 mg/L and an adsorbent dosage of 0.05 g, the effect of initial solution pH on the adsorption behavior of both MOFs materials was systematically investigated (Fig. 10).

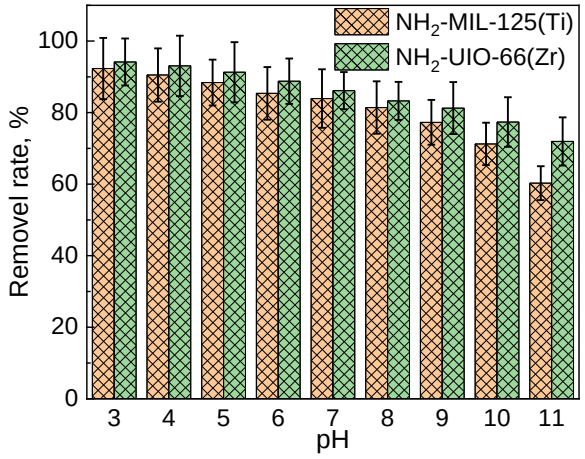

Fig. 10. Effect of initial pH on the adsorption of phosphate by NH_2-MIL-125(Ti) and NH_2-UIO-66(Zr)

When the solution pH was adjusted to 3, the phosphate removal efficiencies of NH_2-MIL-125(Ti) and NH_2-UIO-66(Zr) reached 92.34 % and 94.16 %, respectively, indicating that an acidic environment favors phosphate fixation. This enhancement can be attributed to the protonation of amino groups (-NH_2) into -NH_3+ under low pH conditions, which introduces additional positively charged sites and strengthens electrostatic interactions with phosphate anions. As the pH increased, the removal efficiency gradually declined. At pH 11, the removal rates of NH_2-MIL-125(Ti) and NH_2-UIO-66(Zr) decreased to 60.28 % and 71.94 %, respectively. This reduction is primarily due to two factors: electrostatic repulsion between the increasingly negatively charged adsorbent surface and phosphate ions, and the competitive inhibition of active sites by a high concentration of OH- ions. Notably, NH_2-UIO-66(Zr) consistently outperformed NH_2-MIL-125(Ti) across the pH range, maintaining a removal efficiency approximately 11.5 % higher at pH 11, which suggests that NH_2-UIO-66(Zr) possesses superior tolerance to pH fluctuations. Here, the pH range is set to 3-11 (exceeding the actual water pH range of 6-8), mainly to evaluate the stability and adsorption capacity of MOFs in water quality mutation scenarios (such as acid rain, industrial wastewater discharge) through extreme pH experiments. In addition, it is also used to quickly screen MOFs that still have high adsorption capacity under nonneutral conditions, providing a basis for material selection in practical applications (such as prioritizing the use of wide pH stable MOFs).

The time-dependent phosphate adsorption behavior of NH_2-MIL-125(Ti) and NH_2-UIO-66(Zr) is illustrated in Fig. 11.

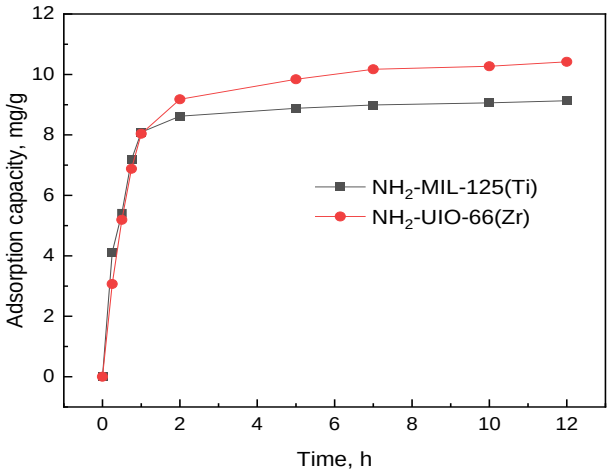

Fig. 11. Effect of adsorption time on the adsorption of phosphate by NH_2-MIL-125(Ti) and NH_2-UIO-66(Zr)

For both MOFs materials, the adsorption capacity per unit mass increased over time and can be divided into two distinct phases: a rapid adsorption phase followed by a slower adsorption phase, with the entire process reaching equilibrium within approximately 7 hours. In the initial stage, the abundance of available surface active sites and minimal mass transfer resistance result in a high adsorption rate. As the reaction progresses, the phosphate concentration in solution decreases and the active sites become progressively occupied, leading to a marked reduction in adsorption rate until equilibrium is reached at which point most accessible adsorption sites are exhausted. Notably, NH_2-MIL-125(Ti) exhibited a higher initial adsorption rate within the first hour compared to NH_2-UIO-66(Zr). However, at equilibrium, NH_2-UIO-66(Zr) demonstrated a superior maximum adsorption capacity. Under identical experimental conditions, the equilibrium adsorption capacities of NH_2-MIL-125(Ti) and NH_2-UIO-66(Zr) were 9.13 mg/g and 10.42 mg/g, respectively, indicating that NH_2-UIO-66(Zr) possesses a higher phosphate uptake capacity. This enhanced performance is attributed to its unique octahedral pore structure and the presence of Zr-O coordination sites, which can form more stable chemical interactions with phosphate ions, thereby facilitating greater adsorption.

To gain deeper insights into the adsorption process, the phosphate adsorption kinetics of the two MOFs materials were investigated. The results revealed that NH_2-MIL-125(Ti) exhibited a relatively rapid adsorption rate, reaching equilibrium within a shorter time frame. This can be attributed to its more open three-dimensional porous structure, which facilitates the fast diffusion of phosphate

ions to the available adsorption sites. In contrast, although NH_2-UIO-66(Zr) showed a slower adsorption rate, it achieved a higher ultimate adsorption capacity, suggesting that its adsorption process involves more complex chemical interactions and ion-exchange mechanisms. To model the adsorption kinetics, both pseudo-first-order and pseudo-second-order models were applied, with the fitted curves shown in Fig. 12 and the corresponding regression coefficients listed in Table 3.

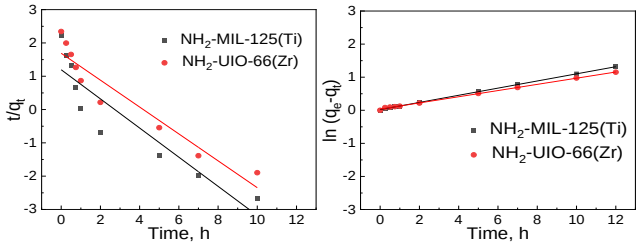

a b

Fig. 12. Fit curves of phosphate adsorption kinetics of the two MOFs materials: a – pseudo first order kinetics; b – pseudo second order kinetics

Under an initial phosphate concentration of 5 mg/L, the coefficient of determination (R^2) for the pseudo-second-order model reached 0.9995 for NH_2-MIL-125(Ti) and 0.9962 for NH_2-UIO-66(Zr), significantly outperforming those of the pseudo-first-order model (both $R^2 < 0.85$). Moreover, the equilibrium adsorption capacities predicted by the pseudo-second-order model (9.36 mg/g and 10.84 mg/g) closely matched the experimentally measured values (9.13 mg/g and 10.42 mg/g). These findings indicate that the phosphate adsorption process is better described by the pseudo-second-order kinetic model, implying that chemisorption is the dominant mechanism.

Langmuir and Freundlich isotherm models are commonly employed to characterize adsorption behavior. In this study, both models were applied to perform nonlinear regression fitting of the experimental data. The fitted curves are shown in Fig. 13, and the corresponding model parameters are summarized in Table 4.

The results indicate that the coefficient of R^2 for the Freundlich model reached 0.9943 and 0.9984 for NH_2-MIL-125(Ti) and NH_2-UIO-66(Zr), respectively, significantly higher than the R^2 values obtained from the Langmuir model (0.9583 and 0.8881). These findings suggest that phosphate adsorption on both MOFs is better described by a multilayer adsorption mechanism, likely governed by the synergistic effects of physical and chemical interactions. Additionally, both materials exhibited 1/n values close to 0.6, indicating that the adsorption process is spontaneous and energetically favorable.

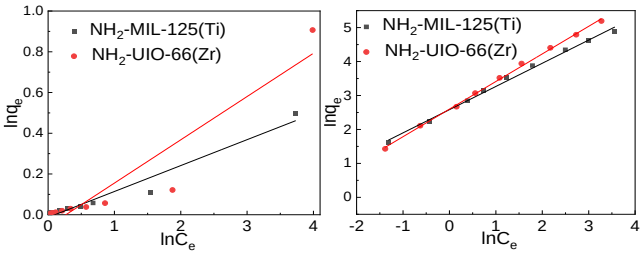

a b

Fig. 13. The fitting of adsorption isotherms of phosphorus by NH_2-MIL-125(Ti) and NH_2-UIO-66(Zr): a – Langmuir model fitting; b – Freundlich model fitting

A comparison of the maximum adsorption capacities (Qm) further revealed that NH_2-UIO-66(Zr) achieved a higher Qm of 203.79 mg/g, surpassing that of NH_2-MIL-125(Ti) (189.63 mg/g) by approximately 14.16 mg/g.

3.4. Regeneration performance analysis

The regeneration performance of NH_2-MIL-125(Ti) and NH_2-UIO-66(Zr) was evaluated through five consecutive adsorption-desorption cycles, with the results presented in Fig. 14.

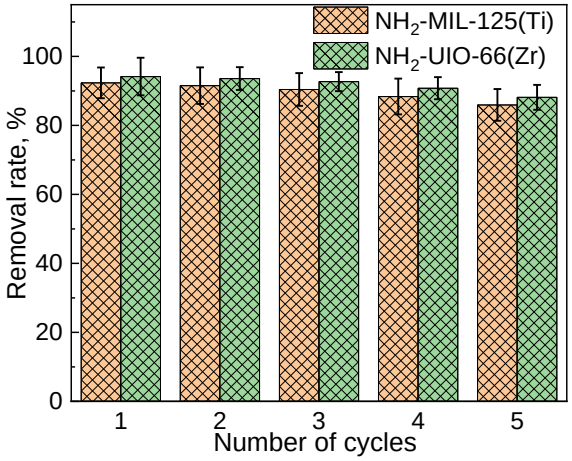

Fig. 14. Adsorption and regeneration properties of NH_2-MIL-125(Ti) and NH_2-UIO-66(Zr)

The data show that the phosphate removal efficiency of both MOFs materials gradually declined with increasing regeneration cycles. For NH_2-MIL-125(Ti), the removal efficiency decreased from 92.34 % in the first cycle to 85.93 % in the fifth.

Table 3. Kinetic correlation coefficients of NH_2-MIL-125(Ti) and NH_2-UIO-66(Zr)

Materials	C_0, mg/L	q_e, mg/g	Pseudo first order kinetics			Pseudo second order kinetics		
			q_e, mg/g	k_1, g/mg/h	R^2	q_e, mg/g	k_2, g/mg/h	R^2
NH_2-MIL-125(Ti)	5	9.13	8.58	0.2914	0.8514	9.36	0.6372	0.9995
NH_2-UIO-66(Zr)	5	10.42	9.37	0.2637	0.9137	10.84	0.6849	0.9986

Table 4. Isothermal correlation coefficients of NH_2-MIL-125(Ti) and NH_2-UIO-66(Zr)

Materials	Langmuir model			Freundlich model		
	Qm, mg/g	KL, L/mg	R^2	KF, $mg^{1-n} \cdot L^n/g$	1/n	R^2
NH_2-MIL-125(Ti)	203.79	0.06725	0.9583	21.5821	0.6835	0.9943
NH_2-UIO-66(Zr)	189.63	0.06092	0.8881	18.7694	0.8132	0.9984

Similarly, NH_2-UIO-66(Zr) exhibited a reduction from 94.16 % to 88.14 % over the same period. Despite this gradual decline, both materials maintained phosphate removal efficiencies above 85 % after five cycles, highlighting their excellent regeneration capability and potential for repeated use in practical water treatment applications.

3.5. Discussion

This study provides valuable insights into the water quality dynamics of reclaimed water-supplemented rivers and the potential application of MOFs for phosphorus removal. The SWMM-EFDC model simulations highlighted the limitations of solely relying on reclaimed water supplementation to meet water quality standards, particularly for NH_3-N and TP. While the reclaimed water effectively reduced COD levels, the persistently high concentrations of NH_3-N and TP necessitate additional treatment strategies. These findings align with previous research [4, 5] that emphasizes the need for integrated approaches in managing water quality in reclaimed water-fed systems.

The successful synthesis and characterization of NH_2-MIL-125(Ti) and NH_2-UIO-66(Zr) demonstrate the potential of MOFs as effective adsorbents for phosphorus removal. The high surface areas and thermal stability of these MOFs, as confirmed by BET and TGA analyses, are consistent with the reported properties of similar MOF materials [22, 23]. The adsorption experiments revealed that NH_2-UIO-66(Zr) exhibited a higher phosphorus adsorption capacity (10.42 mg/g) compared to NH_2-MIL-125(Ti) (9.13 mg/g). This difference could be attributed to the unique octahedral pore structure and the presence of Zr-O coordination sites in NH_2-UIO-66(Zr), which may facilitate stronger chemical interactions with phosphate ions [25].

The adsorption kinetics and isotherm studies further support the potential of these MOFs for phosphorus removal. The pseudo-second-order kinetic model fit suggests that chemisorption is the dominant mechanism, which is consistent with other studies on MOF-based phosphorus adsorption [24]. The Freundlich isotherm model fit indicates a multilayer adsorption process, implying the synergistic effects of physical and chemical interactions. The high regeneration efficiencies (> 85 % after five cycles) of both MOFs highlight their potential for long-term application in water treatment systems.

Compared to traditional phosphorus removal techniques such as chemical precipitation and biological treatment [18, 19], MOF-based adsorption offers several advantages, including simple operation, high adsorption capacity, and good regenerability. While chemical precipitation generates a large amount of sludge and biological methods have strict requirements for C/P ratio, MOFs can effectively remove phosphorus without these limitations. The synergistic effect of MOF adsorption and water replenishment engineering should be fully utilized in the treatment of actual river water quality. Water replenishment projects can improve the ecological flow of rivers and restore the self purification capacity of aquatic ecosystems by increasing water volume, diluting pollutants, and enhancing water mobility. Meanwhile, MOFs with efficient adsorption performance can be added to key polluted areas to reduce excessive total phosphorus pollutants in the short term. Specifically, after the water replenishment project increases the water volume, if the pollutant concentration still exceeds the standard (such as TP > 0.2 mg/L), the standard discharge of river water can be achieved by adding MOFs adsorbent.

However, further research is needed to address the challenges associated with the practical application of MOFs in water treatment. These challenges include the cost-effective synthesis of MOFs, the long-term stability of MOFs in complex water matrices, and the potential for competition from other ions [23]. Future studies should focus on optimizing the synthesis process, evaluating the performance of MOFs in real-world water samples, and developing efficient regeneration strategies.

4. CONCLUSIONS

This study focused on water quality modeling and phosphorus pollution control in reclaimed-water-supplemented rivers, yielding the following key conclusions:

1. A coupled SWMM-EFDC model was developed to simulate the water quality of the Xinfeng River under various reclaimed water supplementation scenarios. Model predictions, validated against field monitoring data, demonstrated the effects of reclaimed water inflow on key water quality parameters, including COD, NH_3-N, and TP. The results indicated that, under the specified inflow conditions, COD concentrations could consistently meet Class V water quality standards, whereas NH_3-N and TP concentrations failed to comply.
2. NH_2-MIL-125(Ti) and NH_2-UIO-66(Zr) were successfully synthesized and characterized using SEM, FTIR, XRD, BET, and TGA to evaluate their morphology, structure, and physicochemical properties. The BET surface areas of NH_2-MIL-125(Ti) and NH_2-UIO-66(Zr) were determined to be 1218.6 m^2/g and 1145.0 m^2/g, respectively, indicating well-developed porous structures that provide abundant active sites for phosphate adsorption. Both materials also exhibited good thermal stability.
3. In phosphate adsorption experiments, NH_2-UIO-66(Zr) demonstrated a higher adsorption capacity (10.42 mg/g) compared to NH_2-MIL-125(Ti) (9.13 mg/g). The adsorption kinetics of both materials were better described by the pseudo-second-order model, with R^2 values of 0.9995 and 0.9986, respectively, and their adsorption isotherms were more consistent with the Freundlich model (R^2 = 0.9943 for NH_2-MIL-125(Ti) and 0.9984 for NH_2-UIO-66(Zr)). Moreover, both MOFs exhibited excellent regeneration performance, maintaining phosphate removal efficiencies above 85 % after five adsorption-desorption cycles.

This study provides valuable insights into the water quality dynamics of reclaimed water-supplemented rivers and demonstrates the potential of MOFs for effective phosphorus removal, contributing to the development of sustainable water management strategies.

Acknowledgments

This work was supported by the Water Ecological Restoration Project of the Anding Section of Dalong River, Daxing District, Beijing (Project No. S110000A001035296003).

REFERENCES

1. **Li, X., Li, X., Li, Y.** Research on Reclaimed Water from the Past to the Future: A Review *Environment Development and Sustainability* 24 (1) 2022: pp. 112 – 137. https://doi.org/10.1007/s10668-021-01495-w
2. **Shan, X., Li, C.G., Li, F.M.** Water Quality Variation of a Typical Urban Landscape River Replenished with Reclaimed Water *Water Cycle* 4 2023: pp. 137 – 144. https://doi.org/10.1016/j.watcyc.2023.04.001
3. **Li, Z., Sun, Z., Zhang, L., Zhan, N., Lou, C., Lian, J.** Investigation of Water Quality and Aquatic Ecological Succession of a Newly Constructed River Replenished by Reclaimed Water in Beijing *Heliyon* 9 (6) 2023: pp. e17045. https://doi.org/10.1016/j.heliyon.2023.e17045
4. **Shi, X., Wang, L., Chen, A., Yu, W., Liu, Y., Huang, X., Long, X., Du, Y., Qu, D.** Enhancing Water Quality and Ecosystems of Reclaimed Water-Replenished River: A Case Study of Dongsha River, Beijing, China *Science of the Total Environment* 926 2024: pp. 172024. https://doi.org/10.1016/j.scitotenv.2024.172024
5. **Zhang, J., Wei, Z., Jia, H., Huang, X.** Factors Influencing Water Quality Indices in a Typical Urban River Originated with Reclaimed Water *Frontiers of Environmental Science & Engineering* 11 (4) 2017: pp. 1 – 10. https://doi.org/10.1007/s11783-017-0943-5
6. **Mano, H., Takeda, F., Kitamura, T., Okamoto, S., Suzuki, Y., Park, C.B., Yasui, N., Kobayashi, K., Tanaka, Y., Yamashita, N., Minamiyama, M.** Water Quality Comparison of Secondary Effluent and Reclaimed Water to Ambient River Water of Southern Okinawa Island Via Biological Evaluation *Environmental Monitoring and Assessment* 189 (9) 2017: pp. 1 – 14. https://doi.org/10.1007/s10661-017-6160-7
7. **Song, K., Lu, Y., Dao, G., Chen, Z., Wu, Y., Wang, S., Liu, J., Hu, H.Y.** Reclaimed Water for Landscape Water Replenishment: Threshold Nitrogen and Phosphorus Concentrations Values for Bloom Control *Algal Research-Biomass Biofuels and Bioproducts* 62 2022: pp. 102608. https://doi.org/10.1016/j.algal.2021.102608
8. **Yan, H., Liu, J.H., Lu, Y., Wu, Y.H., Chen, Z., Hu, H.Y.** Do All Algae Grow Faster in Environments Replenished by Reclaimed Water? Examples of Two Effluents Produced in Beijing *Science of the Total Environment* 919 2024: pp. 170784. https://doi.org/10.1016/j.scitotenv.2024.170784
9. **Zhu, Z., Wang, Z., Yu, Y., Tan, L., Suo, S., Zhu, T., Xu, C., Liu, C., Qin, Y., Liang, W.** Occurrence Forms and Environmental Characteristics of Phosphorus in Water Column and Sediment of Urban Waterbodies Replenished by Reclaimed Water *Science of the Total Environment* 888 2023: pp. 164069. https://doi.org/10.1016/j.scitotenv.2023.164069
10. **Lin, X., Li, S., Sun, D., Zhou, W., Wei, J., Fang, H., Zhu, L., Lu, Z., Xu, J.** Assessment and Comprehensive Evaluation of Large-Scale Reclaimed Water Reuse for Urban River Restoration and Water Resource Management: A Case Study in China *Water* 15 (22) 2023: pp. 3909. https://doi.org/10.3390/w15223909
11. **Zheng, X.N., Wu, D.X., Huang, C.Q., Wu, Q.Y., Guan, Y.T.** Impacts of Hydraulic Retention Time and Inflow Water Quality on Algal Growth in a Shallow Lake Supplied with Reclaimed Water *Water Cycle* 3 2022: pp. 71 – 78. https://doi.org/10.1016/j.watcyc.2022.04.004
12. **Obin, N., Tao, H., Ge, F., Liu, X.** Research on Water Quality Simulation and Water Environmental Capacity in Lushui River Based on Wasp Model *Water* 13 (20) 2021: pp. 2819. https://doi.org/10.3390/w13202819
13. **Barzegar, R., Aalami, M.T., Adamowski, J.** Short-Term Water Quality Variable Prediction Using a Hybrid Cnn-Lstm Deep Learning Model *Stochastic Environmental Research and Risk Assessment* 34 (2) 2020: pp. 415 – 433. https://doi.org/10.1007/s00477-020-01776-2
14. **Bai, J., Zhao, J., Zhang, Z., Tian, Z.** Assessment and a Review of Research on Surface Water Quality Modeling *Ecological Modelling* 466 2022: pp. 109888. https://doi.org/10.1016/j.ecolmodel.2022.109888
15. **Qi, J., Zhang, X., Yang, Q., Srinivasan, R., Arnold, J.G., Li, J., Waldholf, S.T., Cole, J.** Swat Ungauged: Water Quality Modeling in the Upper Mississippi River Basin *Journal of Hydrology* 584 2020: pp. 124601. https://doi.org/10.1016/j.jhydrol.2020.124601
16. **Hwang, S., Jun, S.M., Song, J.H., Kim, K., Kim, H., Kang, M.S.** Application of the Swat-Efdc Linkage Model for Assessing Water Quality Management in an Estuarine Reservoir Separated by Levees *Applied Sciences-Basel* 11 (9) 2021: pp. 3911. https://doi.org/10.3390/app11093911
17. **Kadam, P., Sen, D.** Flood Inundation Simulation in Ajoy River Using Mike-Flood *ISH Journal of Hydraulic Engineering* 18 (2) 2012: pp. 129 – 141. https://doi.org/10.1080/09715010.2012.695449
18. **Ramasahayam, S.K., Guzman, L., Gunawan, G., Viswanathan, T.** A Comprehensive Review of Phosphorus Removal Technologies and Processes *Journal of Macromolecular Science Part a-Pure and Applied Chemistry* 51 (6) 2014: pp. 538–545. https://doi.org/10.1080/10601325.2014.906271
19. **Izadi, P., Andalib, M.** Anaerobic Zone Functionality, Design and Configurations for a Sustainable EBPR Process: A Critical Review *Science of the Total Environment* 870 2023: pp. 162018. https://doi.org/10.1016/j.scitotenv.2023.162018
20. **Yang, L., Jin, X., Hu, Y., Zhang, M., Wang, H., Jia, Q., Yang, Y.** Technical Structure and Influencing Factors of Nitrogen and Phosphorus Removal in Constructed Wetlands *Water Science and Technology* 89 (2) 2024: pp. 271 – 289. https://doi.org/10.2166/wst.2023.414
21. **Zahed, M.A., Salehi, S., Tabari, Y., Farraji, H., Ataei-Kachooei, S., Zinatizadeh, A.A., Kamali, N., Mahjouri, M.** Phosphorus Removal and Recovery: State of the Science and Challenges *Environmental Science and Pollution Research* 29 (39) 2022: pp. 58561–58589. https://doi.org/10.1007/s11356-022-21637-5
22. **Gao, D., Ji, H., Li, R., Munir, M.T., Wu, X., Huang, Y., Li, B.** Advancing Sustainable Phosphorus Removal and Recovery with Metal-Organic Frameworks (MOFs) *Chemical Engineering Journal* 475 2023: pp. 145949. https://doi.org/10.1016/j.cej.2023.145949
23. **Zhang, P., He, M., Huo, S., Li, F., Li, K.** Recent Progress in Metal-Based Composites toward Adsorptive Removal of Phosphate: Mechanisms, Behaviors, and Prospects *Chemical Engineering Journal* 446 (2) 2022: pp. 137081.

https://doi.org/10.1016/j.cej.2022.137081

24. **Xie, Q., Li, Y., Lv, Z., Zhou, H., Yang, X., Chen, J., Guo, H.** Effective Adsorption and Removal of Phosphate from Aqueous Solutions and Eutrophic Water by Fe-Based MOFs of Mil-101 *Scientific Reports* 7 (1) 2017: pp. 3316. https://doi.org/10.1038/s41598-017-03526-x

25. **Wu, Y., Liu, Z., Bakhtari, M.F., Luo, J.** Preparation of Go/Mil-101(Fe,Cu) Composite and Its Adsorption Mechanisms for Phosphate in Aqueous Solution *Environmental Science and Pollution Research* 28 (37) 2021: pp. 51391 – 51403. https://doi.org/10.1007/s11356-021-14206-9